

Use of the small punch test for the estimation of ductile-to-brittle transition temperature shift of irradiated steels

E. Altstadt^{*}, F. Bergner, M. Houska

Helmholtz-Zentrum Dresden-Rossendorf, Bautzner Landstrasse 400, 01328 Dresden, Germany

ARTICLE INFO

Keywords:

Small punch test
Ductile-to-brittle-transition temperature
Reactor pressure vessel steel
Neutron irradiation
Annealing

ABSTRACT

The small punch test is evaluated as a screening procedure for irradiation embrittlement of reactor pressure vessel steels. In particular, the correlation between ductile-to-brittle transition temperatures obtained from this small specimen test technique and from the standard Charpy impact test is investigated. Small punch tests and Charpy impact tests at different temperatures were performed on various steels including materials from original reactor pressure vessels in the unirradiated, neutron irradiated and annealed condition. It is demonstrated that the small punch test is a reliable and effective supportive means for the estimation of the irradiation-induced shift of the ductile-to-brittle transition temperature. It was found that a tanh-fit of the normalized small punch energy in dependence of temperature is preferable in comparison to the two-curve fit of the total small punch energy.

1. Introduction

The small punch (SP) test has been established as a small specimen test technology to support development and monitoring of structural materials [1–6]. It yields estimations of mechanical properties with small amounts of material and is therefore an appropriate means for screening.

So far, the SP test was used for the evaluation of the ductile-to-brittle transition temperature (DBTT) [1,2,4] yield stress [7–11] ultimate tensile stress [9,12–17] fracture toughness [18–20] fatigue [21] and creep properties [22–29]. Various works analysed the distribution of stress and plastic strain in a SP disc by means of analytical modelling [30,31] and by finite element calculations to support the estimation of mechanical properties [8,15,16,32,33]. Abendroth and Kuna applied ductile damage mechanics to the modelling of the SP test and used neural networks for the identification of the parameters of the Guron–Tvergaard–Needleman model [18]. Recently the SP test has even been adapted to curved SP specimens to estimate material properties of small tubes [34]. The role of anisotropy and specimen orientation has been studied in [35–37]. Currently, a European standard on SP testing of metallic materials is being elaborated under the auspices of the Comité Européen de Normalisation (CEN/TC-459) [38]. Recently, ASTM has released the standard E3205-20 “Test Method for Small Punch Testing of Metallic Materials”.

For nuclear components, the SP test provides the possibility for an

"SPT metoda pre thermal ageing" =- Guideline for SPT

evaluation of ageing mechanisms, namely radiation-induced hardening and embrittlement and thermal ageing. Major benefits arise from a lower total activity of a SP sample (approximately 1:220 as compared to a Charpy-size specimen) and from the possibility of re-using already tested standard specimens. Indeed, the Slovakian utility VUJE recently included the SP test into their monitoring concept of the nuclear power plant (NPP) Bohunice [39,40]. The shift of the DBTT is a key element of reactor pressure vessel (RPV) embrittlement surveillance [41,42]. It is therefore interesting to evaluate whether the DBTT shift can be reliably measured by means of the SP test.

As for the SP-test-based estimation of the DBTT, T_{SP} , the following simple correlation has long been proposed [1,5]:

$$T_{SP}[K] = \alpha \cdot T_{CVN}[K] \quad (1)$$

where T_{CVN} is the DBTT from the Charpy impact test using standard specimens $10 \times 10 \times 55$ mm with a 2 mm V-notch (so-called CVN specimens). The factor of proportionality α depends on SP geometry, the material class, the fitting procedure for T_{SP} , and the criterion for the definition of T_{CVN} (e.g. T_{41J} , T_{47J} , T_{68J} , $T_{50\%US}$). The factor of proportionality is significantly smaller than one, which is a consequence of the lower constraint in the SP test. Values of $\alpha = 0.32 \dots 0.45$ are reported in the literature [4,5,9].

This paper aims at evaluating a data set of transition temperatures based on the SP test with respect to their correlation with Charpy-based transition temperatures. Two different procedures for the analysis of SP

^{*} Corresponding author.

E-mail address: e.altstadt@hzdr.de (E. Altstadt).

data are applied and compared with one another. Potential benefits for embrittlement monitoring of RPV steels are discussed.

2. Experiments

2.1. Materials

A number of seven different steels were investigated. These materials include bainitic reactor pressure vessel (RPV) steels, base metals (BM) as well as weld metals (WM), and the ferritic-martensitic 9Cr steel P91. The latter material could be included as it is comparable to RPV steels in terms of tensile properties and toughness. Moreover, the experimental program includes different irradiation conditions, namely unirradiated (u), neutron irradiated (i) and neutron irradiated and annealed (ia). The detailed list of materials is given in Table 1 and the chemical compositions in Table 2.

The material 10KhMFT originates from the original RPV of the nuclear power plant Greifswald, unit 4, operated from 1979 to 1990. Within the post mortem investigation program, material was extracted from the vessel wall and extensively characterized [43,47,51]. The extracted trepanns were cut into layers and allowed a through-thickness analysis of the microstructure and the material properties. The different layers of the trepanns represent various irradiation conditions as the neutron fluence changes from 4.4×10^{19} n/cm² ($E > 0.5$ MeV) at the inner side of the wall to 0.9×10^{19} n/cm² at the outer side (irradiation temperature 270 °C) [52,53]. Moreover, as a consequence of the

Table 1
Materials used for the SP and Charpy impact tests.

Material	Product form; heat treatment; extraction location	Irradiation	References
10KhMFT	RPV Greifswald 4, WM, multi-layer beltline weld (SN0.1.4); original RPV manufacturing technology (Izhora), post welding treatment 650–680 °C/15 h; trepanns 4-4 and 4-6, multiple layers from different thickness positions	i, ia	[43,44]
15Kh2MFAA	RPV Greifswald 8, BM, forged ring 3840 × 140 mm; original manufacturing technology (Skoda); ring 031, block 1, centre layer (~half thickness)	u	[45]
22NiMoCr3.7	RPV Biblis C, BM, forged ring \varnothing 5512 × 250 mm; austenitization 870–905 °C/7h/water quenching, tempering 635–655 °C/11 h; layer H (1/4 thickness location)	u	[46]
SST38	RPV Biblis C, WM (NiCrMo1/OP41TT), multi-layer beltline welding; post welding treatment 540–555 °C/59 h, 465 °C/0h, 590–610 °C/21 h, 465 °C/0h, 590–605 °C/11 h; layer V (40 mm from outer surface)	u	[47]
JFL	IAEA reference steel, forged ring \varnothing 5015 × 290 mm, normalisation 880 °C/9h/oil quenching, tempering 640 °C/9h/air cooling, block 1JFL11, layer from half thickness	u	[48,49]
JRQ	IAEA reference steel, hot rolled plate (3000 × 2500 × 225 mm), normalization 900 °C/1h/oil quenching, tempering 665 °C/12 h/air cooling, stress release 620 °C/40 h, block 5JRQ22, layer A1(plate surface), layer M1 (plate centre)	u	[48,49]
P91	Hot rolled pipe \varnothing 360 × 50 mm; normalization 1040–1100 °C/0.5 h/oil quenching, tempering 730–780 °C/1h; layers from mixed thickness locations	u	[50]

welding technology, there are significant through-thickness variations of the chemical composition and of the structure [47]. This means that the different layers can be considered as “different materials” for the purpose of this paper. A subset of the irradiated samples was annealed for 100 h at 475 °C (condition ia). This treatment was proven to induce a recovery of the mechanical properties comparable to the unirradiated condition [51,54]. Table 3 gives an overview of the different layers included in this investigation (e.g. 4-6-02 means unit 4, trepan no. 6, layer 02).

The material 15Kh2MFAA originates from the original RPV of the NPP Greifswald, unit 8, which was not put into operation, i.e. the material is unirradiated. The RPV was produced by SKODA steelworks. For decommissioning, the vessel was cut into large segments of 0.4×1 m [45]. The Chary-V and SPT samples were fabricated from the middle thickness layers of the forged ring 031.

The materials 22NiMoCr3.7 and SST38 were extracted from the original RPV of the NPP Biblis C, which was also never put into operation. Pieces of the RPV wall were delivered to HZDR by ENSI (the Swiss Federal Nuclear Safety Inspectorate) [47].

JFL and JRQ are so-called IAEA reference steels produced by Kawasaki Steel Corporation. These steels were used in numerous international projects and benchmarks. JFL is a low-Cu steel comparable to A508 Cl. 3, while JRQ is similar to A 533B Cl. 1, but with intentionally increased Cu content. In JRQ, the structure varies with thickness location due to the manufacturing process. Lower bainite and tempered martensite was found in the near surface regions, while granular bainite dominates in the centre [48]. Therefore, specimens from two respective layers are investigated (cf. Table 1).

P91 is a ferritic-martensitic Cr-steel for high temperature applications. It is widely used in thermal power plants and belongs to the candidate materials for Gen-IV and fusion reactor components. The P91 samples were manufactured from a hot-rolled and tempered pipe. There was no significant local variation of hardness and structure [50].

2.2. Charpy impact tests

Standard Charpy-V specimens ($10 \times 10 \times 55$ mm, V-notch 2 mm) were tested according to ISO 148-1. An instrumented TIRA WPM P5d300 machine was used (energy 300 J, impact velocity 5.5 m/s, hammer mass 20 kg). The control of test temperature was realized by a combination of liquid N₂ and electrical heating. The test temperature range was from –25 ... 225 °C for the irradiated steels and –150 ... 150 °C for the unirradiated steels. The number of tests per series was $N \geq 10$ (irradiated steels) and $N \geq 15$ (unirradiated steels). The WWER-440 materials (10KhMFT, 15Kh2MFAA) were tested in orientation T-S (according to the Russian standard PNAE G-7-008-86), the other materials in orientation T-L (L – rolling direction, T – transverse direction, S – thickness direction). As RPV steels do not exhibit significant structural anisotropy, the orientation does not affect the DBTT [55].

2.3. Small punch tests

SP specimens of $10 \times 10 \times 0.5$ mm were manufactured from tested or unused Charpy-sized SE(B) specimens. The orientation was T for all materials (normal direction of the SP disc). In case of the unirradiated materials (cf. Table 1), slices of $10 \times 10 \times 0.6$ mm were cut by electrical discharge machining (EDM) and subsequently ground to final thickness of 0.5 ± 0.005 mm with grit 2500. In case of the irradiated materials, grinding was not possible, therefore the surface finish was realized by two EDM post cuts. The final thickness of irradiated SPT samples was 0.54 ± 0.005 mm.

The main parameters of the SP set-up are: punch diameter $d = 2.5$ mm, receiving hole diameter $D = 4$ mm, receiving hole edge radius $R_E = 0.5$ mm (cf. Fig. 1). The edge size is larger than proposed in the upcoming standard [38]. While the effect of the edge size on the estimation of tensile properties (in particular the yield stress) is significant, it can be

Table 2
Chemical compositions in wt% (balance Fe).

Material	C	Si	V	Cr	Mn	Ni	Mo	Al	P	Cu
10KhMFT *	0.04	0.47	0.17	1.36	1.16	0.14	0.46	n.a.	0.047	0.11
15Kh2MFA	0.15	0.30	0.31	2.86	0.45	0.10	0.79	0.014	0.008	0.05
22NiMoCr3.7	0.215	0.20	0.007	0.42	0.91	0.88	0.53	0.018	0.008	0.04
SST38	0.07	0.16	0.004	0.05	1.21	0.95	0.55	0.02	0.011	0.05
JFL	0.17	0.27	0.003	0.16	1.32	0.71	0.50	n.a.	0.011	0.02
JRQ	0.15	0.24	0.004	0.13	1.20	0.81	0.47	n.a.	0.016	0.13
P91	0.116	0.464	0.23	9.50	0.507	0.09	0.91	0.0195	0.0085	n.a.

* average over the filling layers beyond the welding root.

Table 3
Trepan, layers and irradiation conditions of material 10KhMFT.

Trepan Layer	Distance * (mm)	Fluence ($E > 0.5$ MeV) (10^{19} n/cm ²)	Specimens	Conditions
4-4-02	15	4.0	Charpy-V	i
4-6-02	18	3.9	SPT	i and ia
4-4-04	28	3.6	Charpy-V	i
4-6-04	32	3.5	SPT	i and ia
4-4-05	39	3.3	Charpy-V	i
4-4-06	49	3.0	Charpy-V	i
4-4-07	59	2.8	Charpy-V	i
4-6-08	66	2.6	SPT	i and ia
4-4-08	70	2.5	Charpy-V	ia
4-4-09	80	2.3	Charpy-V	i
4-6-10	87	2.1	SPT	ia
4-4-10	90	2.0	Charpy-V	ia
4-4-11	101	1.8	Charpy-V	i
4-6-14	118	1.5	SPT	i and ia
4-4-13	119	1.5	Charpy-V	i
4-6-16	132	1.2	SPT	i and ia
4-4-15	140	1.1	Charpy-V	i

* centre of disc, measured from inner RPV wall surface.

neglected for the estimation of the ductile-to-brittle transition temperature [9]. The punch displacement v was measured by an inductive sensor with an accuracy of ± 1 μ m and corrected for the device compliance. The punch force was measured by means of a load cell placed between the puncher and the cross head of the testing machine with an accuracy of ± 5 N. At least a number of 25 samples were tested per material and condition. In total, >500 SP tests were performed. The test temperatures were in the range from -172 ... $+100$ °C for the irradiated materials and -194 ... $+100$ °C for the unirradiated materials. For each test the force-displacement curve $F(v)$ was recorded and the small punch energy E_{SP} was calculated as integral of $F(v)$ up to maximum force F_m . As an example, Fig. 2 shows $F(v)$ curves of material 10KhMFT at different test temperatures.

2.4. Determination of ductile-to brittle transition temperatures

The DBTT of a Charpy impact test series is determined by means of a tanh-fit of the impact energy as function of test temperature T .

$$E(T) = A + B \cdot \tanh\left[\frac{T - T_0}{C}\right] = \frac{E_{US} + E_{LS}}{2} + \frac{E_{US} - E_{LS}}{2} \cdot \tanh\left[\frac{T - T_0}{C}\right] \quad (2)$$

A , B , C and T_0 are the fitting parameters, E_{US} and E_{LS} are the upper and lower shelf energies. The energy $E(T)$ can either be the absorbed impact energy KV according to ISO 148–1 or the total impact energy W_t

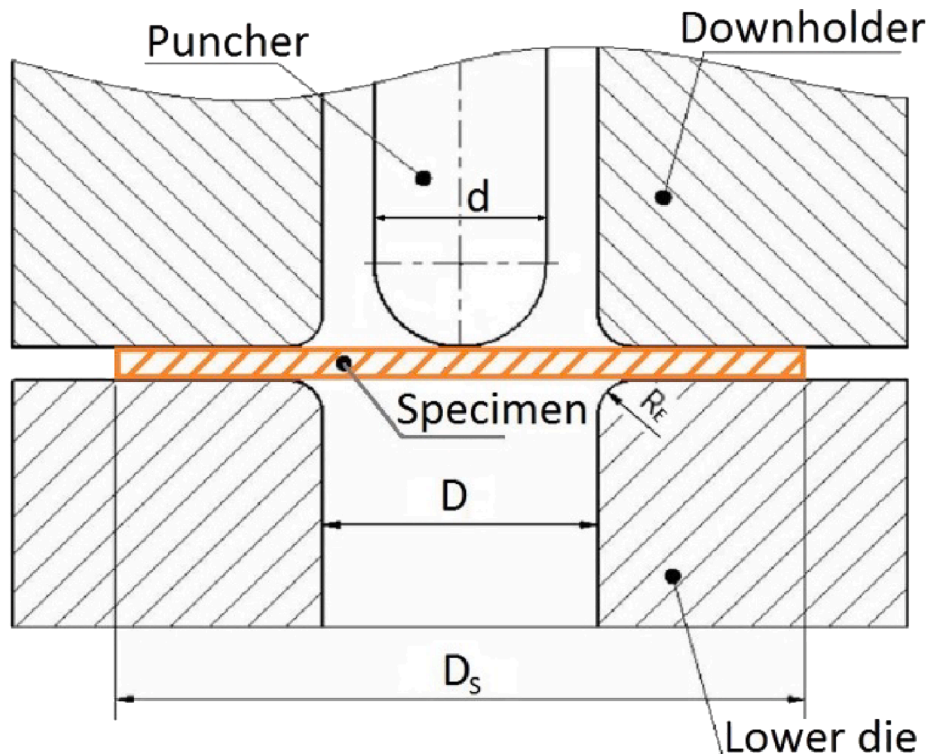


Fig. 1. Geometry of the SPT set-up [37].

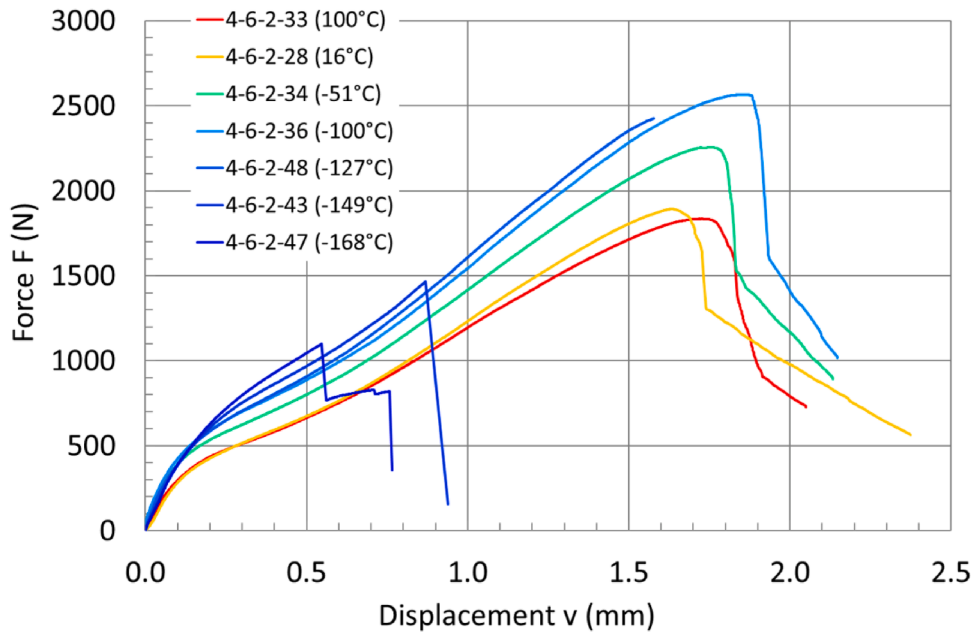


Fig. 2. Force-displacement curves at different temperatures for material 10KhMFT, layer 4-6-02, as irradiated.

calculated as integral of the force-deflection curve $F(s)$. Once the parameters of Eq. (2) are known, we can calculate the transition temperatures T_{41J} and T_{47J} by:

$$T_{41J}|T_{47J} = T_0 + C \cdot \operatorname{atanh} \left[\frac{41J|47J - A}{B} \right] \quad (3)$$

A non-linear iterative least square procedure is used to identify the parameters A , B , C and T_0 . A statistical error estimation for the fit parameters is included [56]. The procedure is implemented in a software package developed at HZDR. Different constraint options are available for the fit, two of them were applied to our data:

- no constraints
- pre-defined lower shelf energy

The standard option is the fit without constraints. The second option can be useful if (i) the standard fit provides a negative lower shelf energy ($E_{LS} < 0$), which is physically meaningless, or if (ii) lower shelf data are missing.

Two fitting methods are available for the determination of the SP-test-based DBTT. The first one is also based on Equation (2). The shift parameter T_0 is directly taken as SP-DBTT ($T_{SP} = T_0$). The normalized energy $E_n = E_{SP}/F_m$ is used for fitting, i.e. $E(T)$ corresponds to E_n [57]. E_{SP} is the area under the force-displacement curve up to the displacement v_m at maximum force F_m [37]. From the definition of E_n and from the shape of the force-displacement curve, it can be concluded that $v_m \leq 2E_n$ holds. Note that the engineering unit of E_n is $\text{mJ/N} = \text{mm}$. The above mentioned fitting constraint (pre-defined lower shelf energy) is especially useful for SP tests of very tough materials where T_{SP} is close to liquid nitrogen temperature or even lower [9].

The second approach for the determination of SP-based DBTT relies on a two-curve exponential fitting of $E_{SP}(T)$ [2,9]:

$$E_{SP,b|d} = A_{b|d} + B_{b|d} \cdot \exp(C_{b|d} \cdot T) \quad (4)$$

where the index “b” refers to the brittle region and the index “d” to the ductile region. A_b , B_b , C_b , A_d , B_d , and C_d are the fitting parameters (A_b , B_b , A_d , $B_d > 0$, $C_b > 0$, $C_d < 0$). The intersection of the two curves $E_{SP,b}(T)$ and $E_{SP,d}(T)$ marks the maximum of the fitted $E_{SP}(T)$ dependency, E_{max} , while the minimum energy is given by $E_{min} = E_{SP}(0 \text{ K})$. The SP transition temperature T_{SP2} is defined as temperature where $E_{SP,b}(T_{SP2}) = 0.5 \times$

($E_{min} + E_{max}$) holds. The index “2” was added to discriminate T_{SP2} (two-curve-fit, Eq. (4)) from T_{SP} (tanh-fit, Eq. (2)).

As an example, Fig. 3 shows the tanh-fit of $E_n(T)$ without constraints for material 10KhMFT, layer 4-6-02. The fitting parameters are: $A = 0.634 \text{ mm}$, $B = 0.366 \text{ mm}$, $C = 40.7 \text{ K}$, $T_{SP} = -129.5 \text{ }^\circ\text{C}$. Fig. 4 shows the two-curve-fit of $E_{SP}(T)$ based on the same data set. The data points were assigned to either $E_{SP,b}$ or $E_{SP,d}$ according to the brittle or ductile fracture appearance of the associated $F(v)$ curve [9] cf. Fig. 2. In Fig. 4, the blue points are associated with $E_{SP,b}$ and the red points with $E_{SP,d}$ (fitting parameters: $A_b = 0.399 \text{ mJ}$, $B_b = 121.3 \text{ mJ}$, $C_b = 0.0157 \text{ K}^{-1}$, $A_d = 1395 \text{ mJ}$, $B_d = 5594 \text{ mJ}$, $C_d = -0.00808 \text{ K}^{-1}$, temperature in K).

Fig. 4 shows that the small punch energy in the ductile range ($E_{SP,d}$) decreases with increasing temperature. This is a consequence of the decreasing yield stress of the material. The normalization leads to an elimination or significant reduction of the decreasing behaviour of the upper shelf since the maximum force is also decreasing with temperature. This makes the tanh-fit applicable to $E_n(T)$.

3. Results

The SP-based and Charpy-based DBTTs are listed in Table 4. For material 10KhMFT, the layers from trepans 4-6 and 4-4 which have a similar thickness position (cf. Table 3) are combined in one row.

The statistical error analysis yielded uncertainties of $|\Delta T_{SP0}| < 10 \text{ K}$ (standard deviation). The DBTTs from Table 4 (translated to Kelvin) were used to determine the correlation coefficient α in Eq. (1) by means of linear regression. Only the complete rows were included. Figs. 5 and 6 show the analyses for the $T_{SP} - T_{47J}$ correlation and for the $T_{SP2} - T_{47J}$ correlation respectively. The factors of proportionality α and associated coefficients of determination R^2 for all combinations of SP-based and Charpy-based DBTTs are listed in Table 5. The tanh-fits of $E_n(T)$ were done without constraints (cf. Section 2.4). If the resulting lower shelf energy was outside the range $0.1 \text{ mm} \leq E_{LS} \leq 0.3 \text{ mm}$, the fit was repeated with a pre-defined lower shelf $E_{LS} = 0.25 \text{ mm}$.

Within the regression analysis it was also checked whether the forced intercept of the $T_{SP} - T_{47J}$ correlation at 0 K according to Eq. (1) is justified. The regression with 2 parameters yielded $T_{SP} = 0.41 \cdot T_{47J} + 3.5 \text{ K}$, hence the absolute offset is negligible.

The obtained correlations were used to evaluate the DBTT of the core weld of the RPV Greifswald unit 4. Fig. 7 shows T_{47J} as a function of the

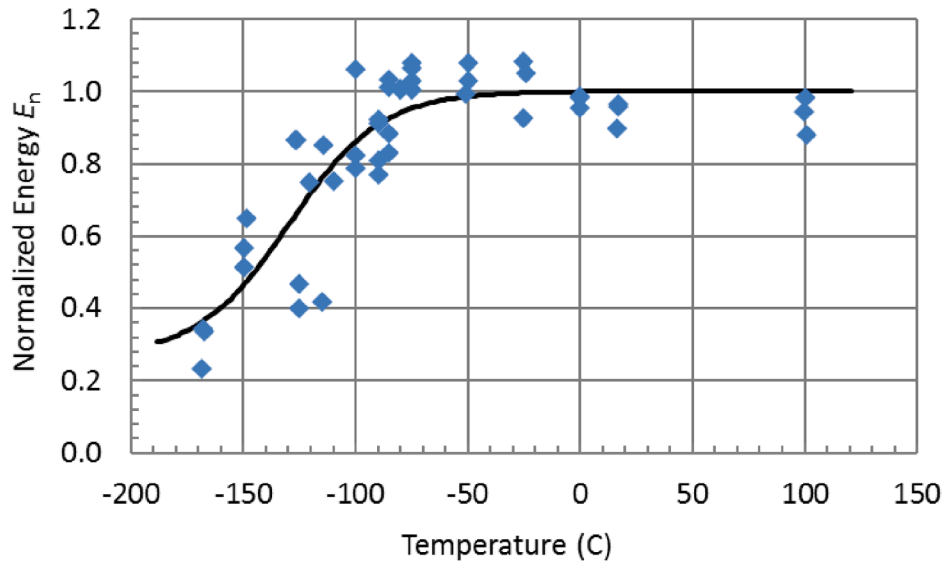


Fig. 3. Tanh-fit of E_n , Eq. (2), for material 10KhMFT, layer 4-6-02, as irradiated, $T_{SP} = -129.5$ °C.

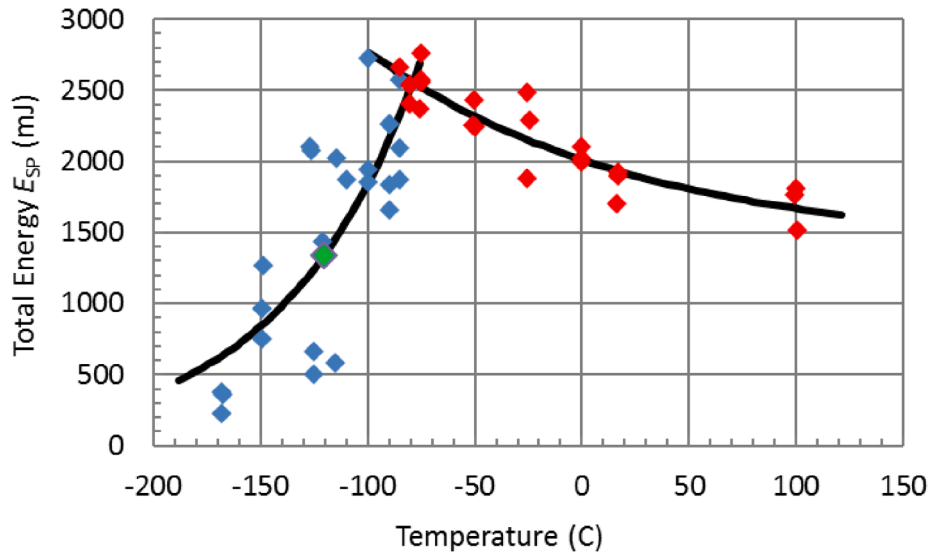


Fig. 4. Two-curve-fit of E_{SP} , Eq. (4), for material 10KhMFT, layer 4-6-02, as irradiated, $T_{SP2} = 120.1$ °C; blue data points used for $E_{SP,b}$, red data point for $E_{SP,d}$. (For interpretation of the references to colour in this figure legend, the reader is referred to the web version of this article.)

thickness position (measured from the inner surface). Both, the values from Charpy impact tests and from SP tests are shown for the irradiated and for the irradiated and annealed condition. The SP based DBTTs were converted to T_{47J} according to Eq. (1) with $\alpha = 0.42$. The T_{SP} values from the tanh-fit were used.

4. Discussion

The correlations between T_{SP} and T_{47J} (T_{41J} , T_0) work surprisingly well (Fig. 5) while the correlations between T_{SP2} and T_{47J} (T_{41J} , T_0) exhibit a larger scatter (Fig. 6). This can also be seen in the corresponding R^2 values. If we consider the CVN based DBTTs as the “true” values and the transformed SP-based values as their predictions, we can define an error as follows:

$$e_{SP,47J} = \left| \frac{T_{SP}[K]}{\alpha_{SP,47J}} - T_{47J}[K] \right| \quad (5)$$

The errors $e_{SP,41J}$, $e_{SP,0}$, $e_{SP2,47J}$, $e_{SP2,41J}$, $e_{SP2,0}$ are defined analogously. The corresponding α values are listed in Table 5. The maximum

and average values of these errors are given in Table 6. The maximum value for the $T_{SP}-T_{47J}$ correlation is $e_{SP,47J} = 16$ K. In Fig. 5, this corresponds to the horizontal distance of the green coloured data point from the regression line (material 15Kh2MFAA, Greifswald 8). This maximum error is small as compared to the usually expected irradiation-induced DBTT shift in RPV steels.

The errors for the correlations based on the two-curve fit (T_{SP2}) are significantly higher. In particular the materials with low DBTTs produce this scatter. Obviously, in case of missing lower shelf data, the two-curve-fit, Eq. (4), is less robust in comparison to the tanh-fit, Eq. (2). The values obtained for the factor of proportionality α range from 0.39 up to 0.44 (cf. Table 5). This is in accordance with values reported in the literature [4,5,9]. Two main factors affect the α -values: the type of Charpy-DBTT (T_{41J} , T_{47J} , T_0) to which the SP-DBTT is correlated, and the fitting method (T_{SP} vs. T_{SP2}).

The application of the $T_{SP}-T_{47J}$ correlation to the core weld of the RPV of NPP Greifswald 4 demonstrates the usability of the SP test for the evaluation of irradiation induced embrittlement. For the as-irradiated condition, Fig. 7 indicates a characteristic through-thickness

Table 4
SP and Charpy based transition temperatures.

Material/Layers/ Condition	T_{SP} (E_n) (°C)	T_{SP2} (E_{SP}) (°C)	T_0 (CVN) (°C)	T_{47J} (CVN) (°C)	T_{41J} (CVN) (°C)
10KhMFT/4-6-02,4-4-02/i	-129.5	-120.1	110.9	72.6	62.5
10KhMFT/4-6-04,4-4-04/i	-142.2	-151.3	43.9	39.3	36.2
10KhMFT/4-4-05/i	-	-	43.5	40.2	38.0
10KhMFT/4-4-06/i	-	-	85.0	75.8	67.7
10KhMFT/4-6-08,4-4-07/i	-102.1	-99.9	128.6	123.4	112.9
10KhMFT/4-4-09/i	-	-	152.3	126.0	116.0
10KhMFT/4-4-11/i	-	-	157.1	134.4	125.8
10KhMFT/4-6-14,4-4-13/i	-111.5	-111.3	129.6	123.8	115.2
10KhMFT/4-6-16,4-4-15/i	-119.9	-120.4	105.7	93.2	87.4
10KhMFT/4-6-02/ia	-159.8	-158.7	-	-	-
10KhMFT/4-6-04/ia	-155.1	-155.8	-	-	-
10KhMFT/4-6-08,4-4-08/ia	-153.0	-151.2	49.9	12.7	6.1
10KhMFT/4-6-10,4-4-10/ia	-148.7	-143.9	38.0	20.6	17.5
10KhMFT/4-4-13/ia	-151.4	-147.9	-	-	-
10KhMFT/4-4-16/ia	-162.1	-151.9	-	-	-
15Kh2MFAA	-172.7	-149.3	-26.3	-50.0	-53.9
22NiMoCr3.7	-174.3	-163.0	-10.4	-37.9	-42.2
SST38	-194.1	-207.3	-58.1	-78.3	-81.4
JFL	-179.5	-176.7	-22.7	-49.9	-53.5
JRQ/layer M1/u	-158.0	-152.9	29.9	15.4	12.4
JRQ/layer A1/u	-185.8	-166.7	-45.2	-75.2	-82.4
P91	-183.0	-178.0	-40.6	-60.3	-62.9

dependence of T_{47J} observed in the Charpy impact test, which exhibits a pronounced minimum close to the welding root. This is nicely reproduced with the SP-based T_{SP} (Fig. 7) for the as-irradiated condition. A similar through-thickness dependence was reported for the fracture toughness (expressed by the reference temperature of the master curve concept) [43,44]. An explanation will be provided below. The recovery of mechanical properties due to the annealing treatment is clearly indicated by significantly lower DBTTs (Fig. 7). Again, the Charpy and SP based values of T_{47J} give a coherent picture. Moreover, the SP test

provides additional information for the layers for which Charpy tests are not available since the material from the trepanns was used up.

In the annealed condition, there is no significant difference between the DBTTs for the welding root (around 35 mm distance from the inner surface, see Fig. 7) and the filling layers (distances beyond 50 mm). This is in contrast to the as-irradiated condition. As the annealed condition can be considered as an equivalent for the unirradiated condition, we can conclude that the particular through-thickness dependence for the as-irradiated DBTTs is caused by irradiation. In particular, the irradiation-induced DBTT shift in the welding root (~ 52 K) is significantly lower as compared to the filling layers (~ 106 K). At a first glance, this behaviour seems to be unexpected as the neutron fluence is decreasing from the inner surface to the outer surface (Section 2.1). Nevertheless, this finding is in line with the through-thickness variation of the Cu content. Cu is known to be the most important impurity element in RPV steels for their susceptibility to irradiation embrittlement. Indeed, the Cu content was reported to be lowest in the welding root [43].

It should be emphasized that this conclusion was possible through the re-use of tested Charpy-sized specimens by means of SP testing. There was no more material left for a complete Charpy impact testing of all layers in the annealed condition. This aspect of the re-use of tested standard samples could also be of general importance for extended RPV surveillance programmes under long term operation. The use of small specimen technologies is a promising option to overcome the lack of surveillance materials [39,40,58,59].

5. Conclusions

It was demonstrated that the SP test can be used as a supportive technique to monitor irradiation embrittlement of RPV steels. The DBTT shift can reliably be estimated based on the correlation between SP-based and Charpy-based transition temperatures (Eq. (1)). The tanh-fit of the normalized SP energy $E_n(T)$ provides a better correlation as compared to the two-curve fit of the total SP energy $E_{SP}(T)$. The SP test is an option for the re-use of tested irradiated standard specimens.

CRedit authorship contribution statement

E. Altstadt: Conceptualization, Methodology, Investigation,

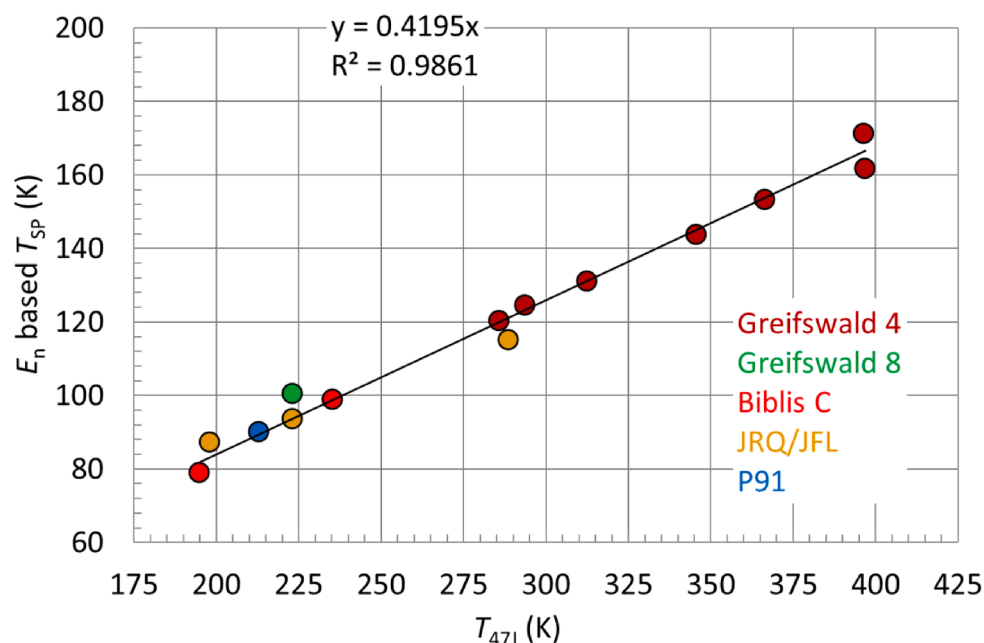


Fig. 5. Correlation between E_n based T_{SP} (tanh-fit) and T_{47J} .

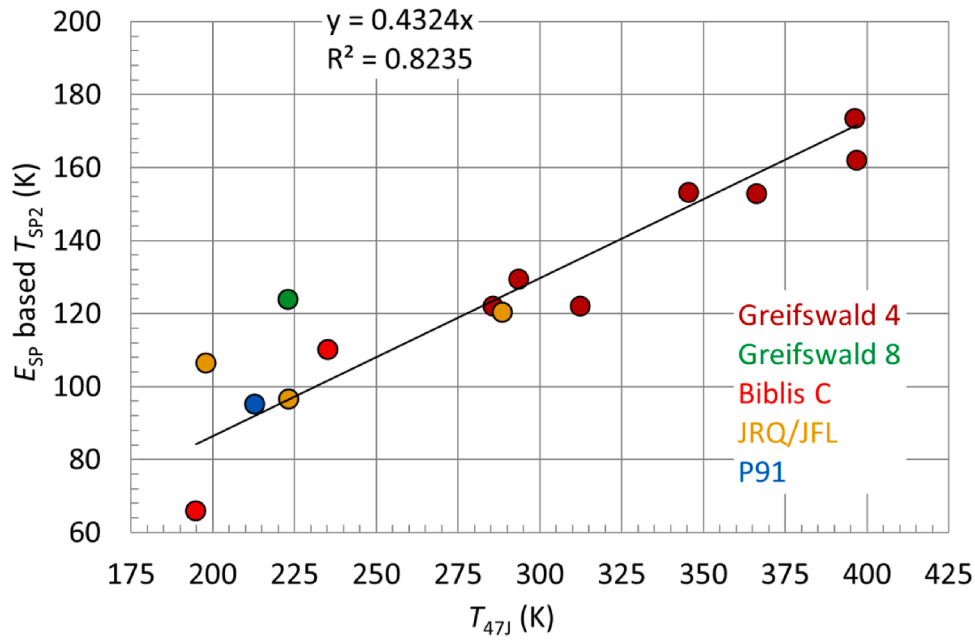


Fig. 6. Correlation between E_{SP} based T_{SP2} (two-curve-fit) and T_{47J} .

Table 5

Factor of proportionality α and coefficient of determination for the correlation between Charpy-based and SP-based DBTTs Eq. (1).

	T_{SP} tanh-fit of $E_n(T)$	T_{SP2} two-curve-fit of $E_{SP}(T)$
T_0 (CVN)	$\alpha = 0.39$ ($R^2 = 0.960$)	$\alpha = 0.41$ ($R^2 = 0.863$)
T_{47J} (CVN)	$\alpha = 0.42$ ($R^2 = 0.986$)	$\alpha = 0.43$ ($R^2 = 0.824$)
T_{41J} (CVN)	$\alpha = 0.43$ ($R^2 = 0.983$)	$\alpha = 0.44$ ($R^2 = 0.813$)

Software, Writing - original draft. **F. Bergner**: Conceptualization, Writing - review & editing, Validation, Formal analysis. **M. Houska**: Methodology, Resources, Investigation.

Table 6

Maximum and average prediction errors (K) over all data points used for the correlation analysis (cf. Table 4) according to Eq. (5).

	$e_{SP,0}$	$e_{SP,47J}$	$e_{SP,41J}$	$e_{SP2,0}$	$e_{SP2,47J}$	$e_{SP2,41J}$
Maximum	36.9	16.0	17.7	55.2	64.9	62.2
Average	12.6	5.8	6.6	19.2	20.1	20.4

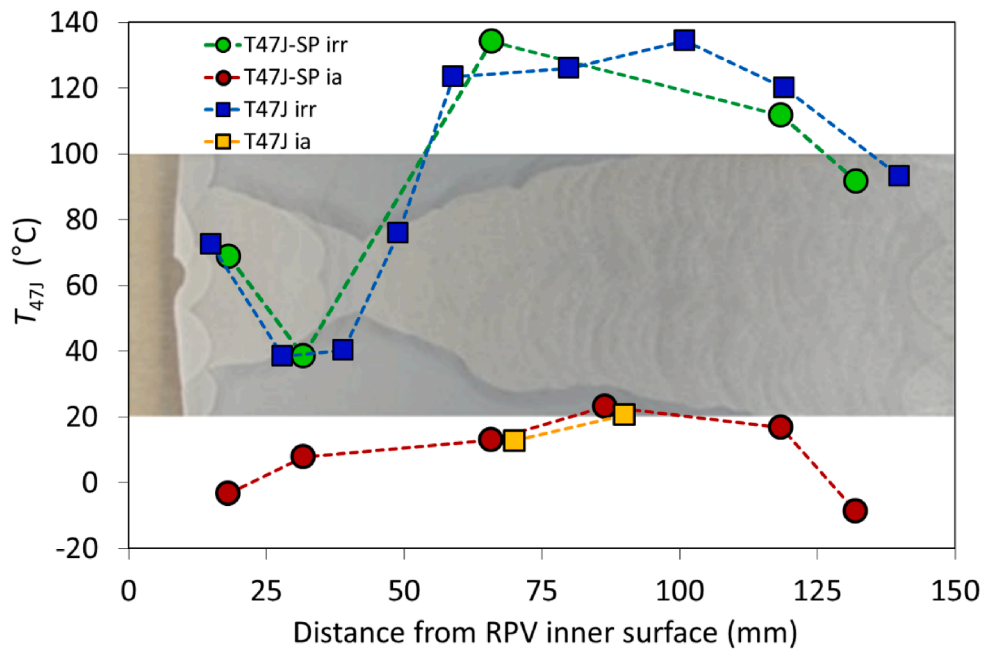


Fig. 7. DBTT T_{47J} obtained from Charpy impact tests and from SP test (recalculated with Eq. (1)) as a function of position in the core welding seam of the RPV of Greifswald unit 4 (material 10KhMFT); as irradiated (irr) and annealed (ia) conditions; the background picture shows the structure of the weld (at the left end the austenitic overlay cladding is visible).

Declaration of Competing Interest

The authors declare that they have no known competing financial interests or personal relationships that could have appeared to influence the work reported in this paper.

Acknowledgements

The work contributes to the Joint Programme on Nuclear Materials (JPNM) within the European Energy Research Alliance (EERA). The work is also an in-kind contribution to the H2020-Euratom project FRACTESUS (grant agreement no. 900014). Specimen preparations by M. Roßner, U. Skorupa and J. Pietzsch and the execution of small punch tests by H. Richter are gratefully acknowledged.

References

- [1] J. Kameda, A kinetic model for ductile-brittle fracture mode transition behavior, *Acta Metall.* 34 (1986) 2391–2398, [https://doi.org/10.1016/0001-6160\(86\)90142-2](https://doi.org/10.1016/0001-6160(86)90142-2).
- [2] T. Misawa, T. Adachi, M. Saito, Y. Hamaguchi, Small punch tests for evaluating ductile-brittle transition behavior of irradiated ferritic steels, *J. Nucl. Mater.* 150 (1987) 194–202, [https://doi.org/10.1016/0022-3115\(87\)90075-4](https://doi.org/10.1016/0022-3115(87)90075-4).
- [3] G.E. Lucas, Review of small specimen test techniques for irradiation testing, *Metall. Trans. A* 21 (1990) 1105–1119, <https://doi.org/10.1007/BF02698242>.
- [4] J. McNaney, G.E. Lucas, G.R. Odette, Application of ball punch tests to evaluating fracture mode transition in ferritic steels, *J. Nucl. Mater.* 179–181 (1991) 429–433, [https://doi.org/10.1016/0022-3115\(91\)90116-O](https://doi.org/10.1016/0022-3115(91)90116-O).
- [5] J.S. Ha, E. Fleury, Small Punch Tests on Steels for Steam Power Plant (I), *KSME Int. J.* 12 (1998) 818–826.
- [6] X. Jia, Y. Dai, Small punch tests on martensitic/ferritic steels F82H, T91 and Optimax-A irradiated in SINQ Target-3, *J. Nucl. Mater.* 323 (2003) 360–367, <https://doi.org/10.1016/j.jnucmat.2003.08.018>.
- [7] J. Kameda, X. Mao, Small-punch and TEM-disc testing techniques and their application to characterization of radiation damage, *J. Mater. Sci.* 27 (1992) 983–989, <https://doi.org/10.1007/BF01197651>.
- [8] E.N. Campitelli, P. Spätig, R. Bonadé, W. Hoffelner, M. Victoria, Assessment of the constitutive properties from small ball punch test: experiment and modeling, *J. Nucl. Mater.* 335 (2004) 366–378, <https://doi.org/10.1016/j.jnucmat.2004.07.052>.
- [9] E. Altstadt, H.E. Ge, V. Kuksenko, M. Serrano, M. Houska, M. Lasan, M. Bruchhausen, J.-M. Lapetite, Y. Dai, Critical evaluation of the small punch test as a screening procedure for mechanical properties, *J. Nucl. Mater.* 472 (2016) 186–195, <https://doi.org/10.1016/j.jnucmat.2015.07.029>.
- [10] J. Calaf Chica, P.M. Bravo Díez, M. Preciado Calzada, Development of an improved prediction method for the yield strength of steel alloys in the Small Punch Test, *Mater. Des.* 148 (2018) 153–166, <https://doi.org/10.1016/j.matdes.2018.03.064>.
- [11] P. Hähner, C. Soyarslan, B. Gülçimen Çakan, S. Bargmann, Determining tensile yield stresses from Small Punch tests: a numerical-based scheme, *Mater. Des.* 182 (2019), 107974, <https://doi.org/10.1016/j.matdes.2019.107974>.
- [12] X. Mao, H. Takahashi, Development of a further-miniaturized specimen of 3 mm diameter for tem disk (ϕ 3 mm) small punch tests, *J. Nucl. Mater.* 150 (1987) 42–52, [https://doi.org/10.1016/0022-3115\(87\)90092-4](https://doi.org/10.1016/0022-3115(87)90092-4).
- [13] R. Hurst, K. Matocha, Where are we now with the European Code of Practice for Small Punch Testing?, in: Proc. 2nd Int. Conf. SSTT “Determination Mech. Prop. Mater. Small Punch Miniat. Test. Tech., Ostrava, Czech Rep., 2012, pp. 4–18.
- [14] K. Kumar, A. Pooleery, K. Madhusoodanan, R.N. Singh, J.K. Chakravarty, R. S. Shrivastaw, B.K. Dutta, R.K. Sinha, Evaluation of ultimate tensile strength using Miniature Disk Bend Test, *J. Nucl. Mater.* 461 (2015) 100–111, <https://doi.org/10.1016/j.jnucmat.2015.02.029>.
- [15] E. Altstadt, M. Houska, I. Simonovski, M. Bruchhausen, S. Holmström, R. Lacalle, On the estimation of ultimate tensile stress from small punch testing, *Int. J. Mech. Sci.* 136 (2018) 85–93, <https://doi.org/10.1016/j.ijmecsci.2017.12.016>.
- [16] J. Calaf Chica, P. Bravo Díez, M. Preciado Calzada, A new prediction method for the ultimate tensile strength of steel alloys with small punch test, *Materials* 11 (2018) 1491, <https://doi.org/10.3390/ma11091491>.
- [17] S. Holmström, I. Simonovski, D. Baraldi, M. Bruchhausen, E. Altstadt, R. Delville, Developments in the estimation of tensile strength by small punch testing, *Theor. Appl. Fract. Mech.* 101 (2019) 25–34, <https://doi.org/10.1016/j.tafmec.2019.01.020>.
- [18] M. Abendroth, M. Kuna, Identification of ductile damage and fracture parameters from the small punch test using neural networks, *Eng. Fract. Mech.* 73 (2006) 710–725, <https://doi.org/10.1016/j.engfractmech.2005.10.007>.
- [19] T. Linse, M. Kuna, J. Schuhknecht, H.-W. Viehrig, Usage of the small-punch-test for the characterisation of reactor vessel steels in the brittle–ductile transition region, *Eng. Fract. Mech.* 75 (2008) 3520–3533, <https://doi.org/10.1016/j.engfractmech.2007.03.047>.
- [20] R. Lacalle, D. Andrés, J.A. Álvarez, F. Gutiérrez-Solana, Transition region of nuclear vessel steels: master curve approach using small punch notched specimens, *Key Eng. Mater.* 734 (2017) 77–86, <https://doi.org/10.4028/www.scientific.net/KEM.734.77>.
- [21] D.T.S. Lewis, R.J. Lancaster, S.P. Jeffs, H.W. Illsley, S.J. Davies, G.J. Baxter, Characterising the fatigue performance of additive materials using the small punch test, *Mater. Sci. Eng. A* 754 (2019) 719–727, <https://doi.org/10.1016/j.msea.2019.03.115>.
- [22] M.L. Saucedo-Muñoz, S.-I. Komazaki, T. Takahashi, T. Hashida, T. Shoji, Creep property measurement of service-exposed SUS 316 austenitic stainless steel by the small-punch creep-testing technique, *J. Mater. Res.* 17 (2002) 1945–1953, <https://doi.org/10.1557/JMR.2002.0288>.
- [23] P. Dymáček, K. Milička, Creep small-punch testing and its numerical simulations, *Mater. Sci. Eng. A* 510–511 (2009) 444–449, <https://doi.org/10.1016/j.msea.2008.06.053>.
- [24] G. Chen, P.C. Zhai, Q.J. Zhang, Creep properties of SUS304 steel by small punch creep tests, *Mater. Sci. Forum.* 631–632 (2009) 387–392, <https://doi.org/10.4028/www.scientific.net/MSF.631-632.387>.
- [25] D. Blagoeva, Y.Z. Li, R.C. Hurst, Qualification of P91 welds through Small Punch creep testing, *J. Nucl. Mater.* 409 (2011) 124–130, <https://doi.org/10.1016/j.jnucmat.2010.09.015>.
- [26] B. Gülçimen, P. Hähner, Determination of creep properties of a P91 weldment by small punch testing and a new evaluation approach, *Mater. Sci. Eng. A* 588 (2013) 125–131, <https://doi.org/10.1016/j.msea.2013.09.029>.
- [27] J. Vivas, C. Capdevila, E. Altstadt, M. Houska, D. San-Martín, Importance of austenitization temperature and ausforming on creep strength in 9Cr ferritic/martensitic steel, *Scr. Mater.* 153 (2018) 14–18, <https://doi.org/10.1016/j.scriptamat.2018.04.038>.
- [28] J. Vivas, C. Capdevila, E. Altstadt, M. Houska, M. Serrano, D. De-Castro, D. San-Martín, Effect of ausforming temperature on creep strength of G91 investigated by means of Small Punch Creep Tests, *Mater. Sci. Eng. A* 728 (2018) 259–265, <https://doi.org/10.1016/j.msea.2018.05.023>.
- [29] J. Vivas, D. De-Castro, E. Altstadt, M. Houska, D. San-Martín, C. Capdevila, Design and high temperature behavior of novel heat resistant steels strengthened by high density of stable nanoprecipitates, *Mater. Sci. Eng. A* 793 (2020), 139799, <https://doi.org/10.1016/j.msea.2020.139799>.
- [30] J. Chakrabarty, A theory of stretch forming over hemispherical punch heads, *Int. J. Mech. Sci.* 12 (1970) 315–325.
- [31] T.S. Byun, E.H. Lee, J.D. Hunn, K. Farrell, L.K. Mansur, Characterization of plastic deformation in a disk bend test, *J. Nucl. Mater.* 294 (2001) 256–266, [https://doi.org/10.1016/S0022-3115\(01\)00484-6](https://doi.org/10.1016/S0022-3115(01)00484-6).
- [32] I. Simonovski, S. Holmström, M. Bruchhausen, Small punch tensile testing of curved specimens: finite element analysis and experiment, *Int. J. Mech. Sci.* 120 (2017) 204–213, <https://doi.org/10.1016/j.ijmecsci.2016.11.029>.
- [33] K. Li, J. Peng, C. Zhou, Construction of whole stress-strain curve by small punch test and inverse finite element, *Results Phys.* 11 (2018) 440–448, <https://doi.org/10.1016/j.rinp.2018.09.024>.
- [34] I. Simonovski, D. Baraldi, S. Holmström, E. Altstadt, R. Delville, M. Bruchhausen, Determining the ultimate tensile strength of fuel cladding tubes by small punch testing, *J. Nucl. Mater.* 509 (2018) 620–630, <https://doi.org/10.1016/j.jnucmat.2018.07.041>.
- [35] N. Okuda, R. Kasada, A. Kimura, Statistical evaluation of anisotropic fracture behavior of ODS ferritic steels by using small punch tests, *J. Nucl. Mater.* 386–388 (2009) 974–978, <https://doi.org/10.1016/j.jnucmat.2008.11.026>.
- [36] E. Altstadt, M. Serrano, M. Houska, A. García-Junceda, Effect of anisotropic microstructure of a 12Cr-ODS steel on the fracture behaviour in the small punch test, *Mater. Sci. Eng. A* 654 (2016) 309–316, <https://doi.org/10.1016/j.msea.2015.12.055>.
- [37] E. Altstadt, F. Bergner, A. Das, M. Houska, Effect of anisotropic microstructure of ODS steels on small punch test results, *Theor. Appl. Fract. Mech.* (2019), <https://doi.org/10.1016/j.tafmec.2019.01.014>.
- [38] M. Bruchhausen, T. Austin, S. Holmström, E. Altstadt, P. Dymacek, S. Jeffs, R. Lancaster, R. Lacalle, K. Matocha, J. Petzová, European standard on small punch testing of metallic materials, in: ASME, 2017: p. V01AT01A065. doi:10.1115/PVP2017-65396.
- [39] J. Petzová, M. Březina, M. Kapusňák, Ľ. Kupča, Application of Small Punch Testing Methods for Thermal Ageing Monitoring at Primary Circuit Components in Nuclear Power Plant, in: Vol. 1A Codes Stand., American Society of Mechanical Engineers, Boston, Massachusetts, USA, 2015: p. V01AT01A063. doi:10.1115/PVP2015-45539.
- [40] M. Březina, J. Petzová, Ľ. Kupča, M. Kapusňák, Utilization of SPT Techniques for Evaluation of Changes in the Properties of the VVER-440 Reactor Pressure Vessel Steels After Their Irradiation in the Research and Power Reactors, in: Vol. 1A Codes Stand., American Society of Mechanical Engineers, Boston, Massachusetts, USA, 2015: p. V01AT01A062. doi:10.1115/PVP2015-45528.
- [41] R.K. Nanstad, M.A. Sokolov, S.R. Ortner, P.D. Styman, Neutron and Thermal Embrittlement of RPV Steels: An Overview, in: W.L. Server, M. Brumovský (Eds.), *Int. Rev. Nucl. React. Press. Vessel Survell. Programs*, ASTM International, 100 Barr Harbor Drive, PO Box C700, West Conshohocken, PA 19428-2959, 2018, pp. 68–106. doi:10.1520/STP160320170063.
- [42] A. Ballesteros, E. Altstadt, F. Gillemot, H. Hein, J. Wagemans, J. Rouden, J. Barthelmes, K. Wilford, M. Serrano, M. Brumovský, R. Chaouadi, S. Ortner, Monitoring radiation embrittlement during life extension periods, *Nucl. Eng. Des.* 267 (2014) 197–206, <https://doi.org/10.1016/j.nucengdes.2013.11.068>.
- [43] H.-W. Viehrig, E. Altstadt, M. Houska, M. Valo, Fracture mechanics characterisation of the beltline welding seam of the decommissioned WWER-440 reactor pressure vessel of nuclear power plant Greifswald Unit 4, *Int. J. Press. Vessels Pip.* 89 (2012) 129–136, <https://doi.org/10.1016/j.ijpvp.2011.10.016>.

- [44] H.-W. Viehrig, M. Houska, E. Altstadt, Radiation and annealing response of WWER 440 beltline welding seams, *J. Nucl. Mater.* 456 (2015) 334–343, <https://doi.org/10.1016/j.jnucmat.2014.10.004>.
- [45] H.-W. Viehrig, M. Scibetta, K. Wallin, Application of advanced master curve approaches on WWER-440 reactor pressure vessel steels, *Int. J. Press. Vessels Pip.* 83 (2006) 584–592, <https://doi.org/10.1016/j.ijpvp.2006.04.005>.
- [46] C. Zurbuchen, Influence of specimen type, crack length and evaluation method on quasi-static and dynamic fracture toughness properties, in: *Proceedings of the ASME 2009 Pressure Vessels and Piping Conference*, 2009, pp. 511–517, <https://doi.org/10.1115/PVP2009-77796>.
- [47] H.-W. Viehrig, M. Houska, D. Kalkhof, H.-J. Schindler, Fracture mechanics characterisation of reactor pressure vessel multi-layer weld metal, *Int. J. Press. Vessels Pip.* 135–136 (2015) 36–51, <https://doi.org/10.1016/j.ijpvp.2015.10.002>.
- [48] H.-W. Viehrig, C. Zurbuchen, Anwendung des Master Curve-Konzeptes zur Charakterisierung der Zähigkeit neutronenbestrahlter Reaktordruckbehälterstähle, HZDR, Dresden, 2007. <https://www.hzdr.de/publications/PublDoc-1973.pdf>.
- [49] C. Zurbuchen, H.-W. Viehrig, F.-P. Weiss, Master Curve and Unified Curve applicability to highly neutron irradiated Western type reactor pressure vessel steels, *Nucl. Eng. Des.* 239 (2009) 1246–1253, <https://doi.org/10.1016/j.nucengdes.2009.03.008>.
- [50] S. Kohlar, Gefüge und Eigenschaften des warmfesten Chromstahls P91, Helmholtz-Zentrum Dresden-Rossendorf, Dresden, 2009. <http://nbn-resolving.de/urn:nbn:de:bsz:d120-qucosa-229778>.
- [51] A. Ulbricht, E. Altstadt, F. Bergner, H.-W. Viehrig, U. Keiderling, Small-angle neutron scattering investigation of as-irradiated, annealed and reirradiated reactor pressure vessel weld material of decommissioned reactor, *J. Nucl. Mater.* 416 (2011) 111–116, <https://doi.org/10.1016/j.jnucmat.2010.12.219>.
- [52] J. Konheiser, U. Rindelhardt, H.-W. Viehrig, B. Boehmer, B. Gleisberg, Pressure Vessel Investigations of the Former Greifswald NPP: Fluence Calculations and Niobium Based Fluence Measurements, in: *Vol. 1 Plant Oper. Maint. Life Cycle Compon. Reliab. Mater. Issues Codes Stand. Licens. Regul. Issues Fuel Cycle High Level Waste Manag.*, ASMEDC, Miami, Florida, USA, 2006, pp. 587–592. doi: 10.1115/ICONE14-89578.
- [53] U. Rindelhardt, H.-W. Viehrig, J. Konheiser, J. Schuhknecht, K. Noack, B. Gleisberg, RPV material investigations of the former VVER-440 Greifswald NPP, *Nucl. Eng. Des.* 239 (2009) 1581–1590, <https://doi.org/10.1016/j.nucengdes.2008.07.018>.
- [54] A. Ulbricht, F. Bergner, J. Böhmert, M. Valo, M.-H. Mathon, A. Heinemann, SANS response of VVER440-type weld material after neutron irradiation, post-irradiation annealing and reirradiation, *Philos. Mag.* 87 (2007) 1855–1870, <https://doi.org/10.1080/14786430601102999>.
- [55] J.-T. Kim, H.-K. Kwon, K.-C. Kim, J.-M. Kim, Improved Mechanical Properties of the A 508 Class 3 Steel for Nuclear Pressure Vessel Through Steelmaking, in: E. Nisbett, A. Melilli (Eds.), *Steel Forg. Second Vol.*, ASTM International, 100 Barr Harbor Drive, PO Box C700, West Conshohocken, PA 19428-2959, 1997, pp. 18–18–15. doi:10.1520/STP16590S.
- [56] P. Urwank, Unambiguous curve fitting and error estimation for charpy impact test data of reactor pressure vessel steels, suitable for a small number of samples, *J. Nucl. Mater.* 161 (1989) 24–29, [https://doi.org/10.1016/0022-3115\(89\)90458-3](https://doi.org/10.1016/0022-3115(89)90458-3).
- [57] M. Bruchhausen, S. Holmström, J.-M. Lapetite, S. Ripplinger, On the determination of the ductile to brittle transition temperature from small punch tests on Grade 91 ferritic-martensitic steel, *Int. J. Press. Vessels Pip.* 155 (2017) 27–34, <https://doi.org/10.1016/j.ijpvp.2017.06.008>.
- [58] M. Scibetta, E. Lucon, R. Chaouadi, E. van Walle, R. Gérard, Use of Broken Charpy V-notch Specimens from a Surveillance Program for Fracture Toughness Determination, *J. ASTM Int.* 3 (2006) 12450, <https://doi.org/10.1520/JAI12450>.
- [59] E. Altstadt, E. Keim, H. Hein, M. Serrano, F. Bergner, H.-W. Viehrig, A. Ballesteros, R. Chaouadi, K. Wilford, FP7 Project LONGLIFE: overview of results and implications, *Nucl. Eng. Des.* 278 (2014) 753–757, <https://doi.org/10.1016/j.nucengdes.2014.09.003>.